

DeepLocalization: Landmark-based Self-Localization with Deep Neural Networks

Nico Engel, Stefan Hoermann, Markus Horn, Vasileios Belagiannis and Klaus Dietmayer

Abstract— We address the problem of landmark-based vehicle self-localization by relying on multi-modal sensory information. Our goal is to determine the autonomous vehicle’s pose based on landmark measurements and map landmarks. The map is built by extracting landmarks from the vehicle’s field of view in an off-line way, while the measurements are collected in the same way during inference. To map the measurements and map landmarks to the vehicle’s pose, we propose DeepLocalization, a deep neural network that copes with dynamic input. Our network is robust to missing landmarks that occur due to the dynamic environment and handles unordered and adaptive input. In real-world experiments, we evaluate two inference approaches to show that DeepLocalization can be combined with GPS-sensors and is complementary to filtering approaches such as an extended Kalman filter. We show that our approach achieves state-of-the-art accuracy and is about ten times faster than the related work.

I. INTRODUCTION

Self-localization is the task of determining the vehicle’s position and orientation (pose) within a coordinate system, based on sensory information [1]. In autonomous driving, the precise vehicle position is essential for path planning [2]. Furthermore, it increases the vehicle’s safety and reliability by incorporating prior information from a digital map for the environment’s perception [3].

The localization accuracy is, of course, subject to the driving environment. In structured and organized environments, e.g. freeways, the localization accuracy can be as low as a couple of meters. Regular global navigation satellite systems (GNSS), e.g. GPS, usually provide sufficient results for localization [4]. Self-localization can additionally contribute to the navigation task. However, more complex and unstructured scenarios in urban and even rural areas demand an extensive environment perception with a precise localization, requiring accuracies in the range of 0.1 m – 0.5 m. Achieving this precision is possible with a dGPS-System that relies on data correction from a network of ground-based reference stations. Due to its high cost it is not a sustainable solution to equip every autonomous driving vehicle with dGPS. In addition, all GNSS’s heavily rely on satellite coverage, which can be poor in cities where the clear sight to the satellites can be concealed by houses and skyscrapers [5]. The most adopted solution in localization is to combine multiple sensors, e.g. radar, camera, laser and GPS, with a high-precision map to estimate the vehicle’s pose [6], [7], [8].

The authors are with Institute of Measurement, Control and Microtechnology, Ulm University, 89081 Ulm, Germany. E-Mail: {firstname.lastname}@uni-ulm.de

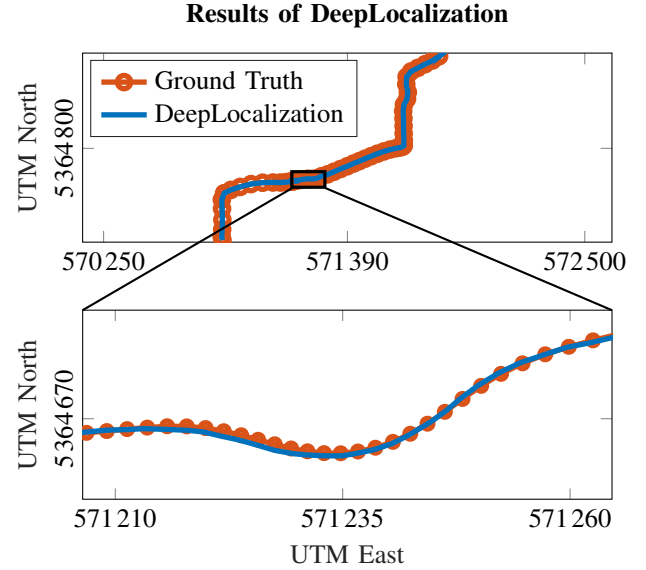


Fig. 1. Results of DeepLocalization. The plot on the top shows an extract from our evaluation sequence, where the red line is the ground truth trajectory and the blue line the output from our network in combination with an EKF. The bottom plot shows an enlarged section of the top trajectory.

Classic probabilistic localization approaches have shown great results in unstructured environments enabling the successful deployment of autonomous vehicles in many cities around the world using either a grid-based representation of the environment [9] or a landmark-based map. In the latter case, the map contains static and easily recognizable objects [10], [11]. In comparison to grid-based maps, where the entire area is discretized into small cells, the storage requirement for 2D landmarks is negligible. Furthermore, landmark-based maps are easier to maintain and update, because landmarks can be added or removed without much effort.

In this work, we present an approach for self-localization based on landmarks. By relying on multi-modal sensor information, we extract a set of landmarks from the vehicle’s field of view and build a map off-line. During localization, the autonomous vehicle extracts landmarks in real-time that are matched with the map landmarks and eventually estimates the vehicle’s pose. Note that there are map landmarks which will not be visible after building the map due to the dynamic environment (e.g. different lighting and weather conditions, infrastructure and dynamic objects). Furthermore, we can only rely on the vehicle’s pose from the previous time-step to estimate the current pose, which adds additional ambiguity

to the pose estimation. On top of the environment challenges, we also have to deal with input of dynamic size since the number of landmarks varies over times. As a result, matching the measured landmarks that are extracted in real-time with the map landmarks is not straightforward. To address these issues, we introduce a deep neural network that learns to match the measured landmarks with the map landmarks. Traditional convolutional neural networks are not well-suited for our problem, because they require the input data to be structured. Moreover, transforming the dynamic input into an ordered representation is not trivial.

We derive our motivation from the latest network architectures for 3D unstructured data processing. The recently introduced PointNet architecture [12] copes with unordered point lists. The main idea of PointNet is to create a signature of the dynamic input list, i.e. 3D point cloud, by combining a multi-layer perceptron with the max-pooling operation. We propose a related network architecture that receive input from two dynamic lists to regress the vehicle's pose. The measured landmarks compose one dynamic list and the map landmarks the other one. Moreover, our network learns to regress the relative pose offset between two time-steps instead of the absolute pose. By combining our model with either GPS measurements or a filtering approach, we achieve real-time vehicle self-localization with state-of-the-art accuracies.

In our experiments, we study the performance of our approach on our own data, namely the Ulm-Lehr dataset. First, we perform a number of baseline evaluations to show the generalization capabilities of our approach. Then, we compare our results with prior work to show better localization accuracy and faster inference. Our approach functions in the range of 2ms. In addition, we demonstrate that our algorithm is complementary to filtering approaches by combining it with an extended Kalman filter. We call our approach *DeepLocalization*. Some of our results are shown in Fig. 1.

II. RELATED WORK

Self-Localization is a fundamental problem in robotics for navigation and object manipulation. The standard scenario often is to estimate the robot's pose by accumulating noisy sensor measurements [1], [13], [14], based on a filtering algorithm such as an extended Kalman filter (EKF) or particle filter, i.e. Monte Carlo localization (MCL). Later, self-localization has been raised to a vital task for autonomous driving vehicles too. Several approaches have been proposed the past few years. Below, we discuss the methods that are related to ours as well as deep learning approaches.

Classic Self-Localization. A common way of categorizing the localization methods is based on the type of environment representation. The majority of the approaches relies on grid-based maps, i.e. discretization of the environment into 2D or 3D cells. In that case, the features of the environment are usually generated for every cell and saved in an off-line map. In the on-line phase, the same feature extraction algorithms are used for producing measurements. By aligning the off-line map with the measurements the vehicles pose can

be estimated. Levinson *et al.* [15], [16] have proposed a probabilistic grid, where the remittance value of LiDAR measurements is modeled for each cell as its own Gaussian distribution. Wolcott *et al.* [17] have proposed the Gaussian mixture maps in which each cell of the 2D grid contains Gaussian mixture models over the height (vertical structure), measured by multiple LiDAR scanners. The advantage over the approaches, which use the reflectivity of LiDAR scans, e.g. [16], lies in the robust localization accuracy even in adverse weather conditions. Besides the grid-based environment representation, landmark-based maps are prevalent in autonomous driving applications. The maps usually contain sets of independent 2D or 3D points to represent distinct and recognizable objects. Traditionally, observed point clouds from different sensors are registered to the pre-build map using the iterative closest point algorithm [18] or similar variations [19]. Instead of searching for a single best solution for the registration problem, several approaches use Monte Carlo localization methods in combination with a digital map and sensor measurements to derive the vehicle's pose [11], [20].

Deep Localization. Deep learning approaches have advanced the field of localization in the past few years. Kendall *et al.* have proposed PoseNet [21], a convolutional neural network that regresses the camera's 6 degrees of freedom pose relative to the scene from a single RGB image. A similar approach has been introduced by Valada *et al.* with VLocNet [22]. The goal is to regress the global pose and simultaneously estimate the odometry between two frames. The network is based on residual neural networks that take two consecutive monocular images as input. PointNet [12] uses sets of 3D points to learn a global feature representation of the input which can be used, e.g. for classification and segmentation. Although, PointNet is not suited for processing input from multiple sources, it is related to our model. We propose an architecture related to PointNet within the context of localization that regresses the vehicle's pose from two dynamic input lists, the measurements and map landmarks. Finally, DeepMapping [23] is closer to our approach by aligning point clouds to a global coordinate system. The method regresses the sensor's pose using a deep neural network followed by a mapping network that models the structure of a scene using grid maps. Contrary to this, our model directly learns the alignment transformation from the two dynamic inputs without requiring an intermediate step.

III. METHOD

We consider multi-modal measurements from laser, radar and camera sensors. A set of landmarks is extracted from the raw data, using pre-processing methods for each time-step [11]. All extracted landmarks from the vehicle's field of view are registered to the same coordinate system. This is performed off-line and constitutes our map building process. In general, the map is comprised of 2D points, each resembling a static and recognizable object [1]. In the on-line phase, landmarks, which we refer to as *measurements*, are extracted the same way. Our goal is to localize the vehicle

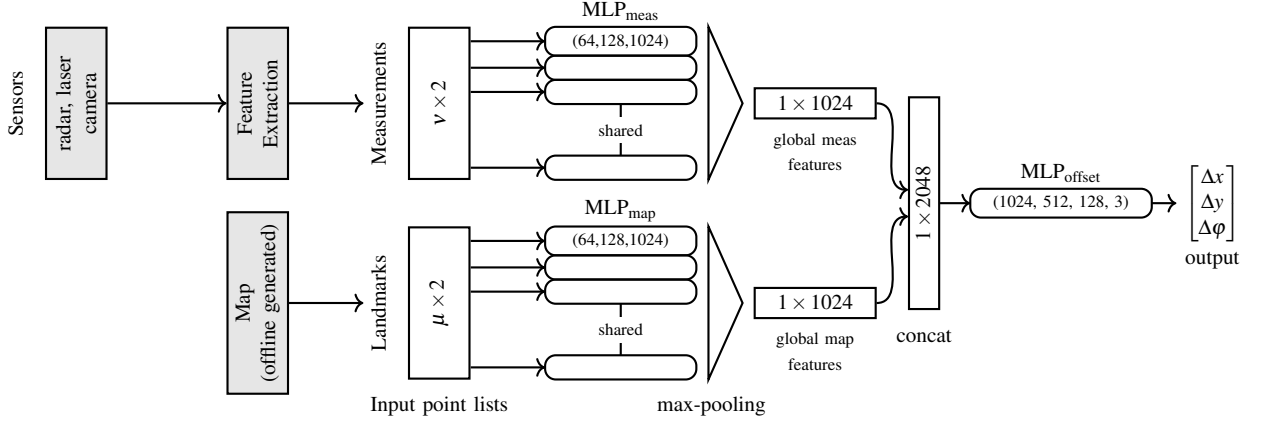


Fig. 2. Network architecture. The raw measurements from the sensors are pre-processed (grey boxes) using feature extraction algorithms. The input points are then transformed into higher dimensional space using independent multi layer perceptron networks for the measurements and map landmarks. The parameters are shared for each input type. A max-pooling operation is performed on the transformed input points resulting in two feature vectors describing the global structure of each point list. The two feature vectors are concatenated and used as input for another multi layer perceptron that estimates a transformation to correct an initial or previous localization result.

w.r.t to the *map landmarks* by utilizing the measurements and the vehicle's initial location. Next, we describe all steps in detail.

A. Problem Definition

We seek for mapping the measurements $\{\mathbf{z}_1, \dots, \mathbf{z}_v\}$ and the map landmarks $\{\mathbf{m}_1, \dots, \mathbf{m}_\mu\}$ to the vehicle's pose $[x, y, \phi]$. However, regressing directly the absolute position in a global coordinate system, such as the Universal Transverse Mercator (UTM) coordinate system, is highly ambiguous. Instead, we propose to regress the pose offset between the previous and current time-step. We make use of the vehicle's pose from the previous (or initial) time-step $t-1$ and the current measurements to predict the pose offset $[\Delta x, \Delta y, \Delta \phi]$ to the current pose. The position offset Δx and Δy can be interpreted as translation and the orientation offset $\Delta \phi$ as rotation.

We present a deep neural network architecture that receives the measurements of the current time-step t and the map landmarks from $t-1$ as input to predict the pose offset between the previous and current time-step. The idea is to learn the relation between measurements and map landmarks to regress the vehicle's pose offset. The proposed mapping is parameterized by θ and is given by:

$$f_\theta(\{\mathbf{z}_1, \dots, \mathbf{z}_v\}_t, \{\mathbf{m}_1, \dots, \mathbf{m}_\mu\}_{t-1}) \rightarrow [\Delta \hat{x}, \Delta \hat{y}, \Delta \hat{\phi}]. \quad (1)$$

Note that we have 2-axis of translation and 1-axis of rotation in our problem, which is a common way of describing an agent's pose [1]. Based on the output of f_θ and the previous vehicle's pose, we can obtain the current pose. This is described by:

$$\mathbf{p}_t = \mathbf{p}_{t-1} + [\Delta \hat{x}, \Delta \hat{y}, \Delta \hat{\phi}]^T, \quad (2)$$

where $\mathbf{p}_t, \mathbf{p}_{t-1} \in \mathbb{R}^3$. We use the UTM coordinate system for localization.

It is important to note that there exists no specific order in which the measurements are obtained. Furthermore, the

amount of landmarks v, μ in each input set is not known in advance and varies over time. The only fixed information are the dimensions of the landmarks $v, \mu \in \mathbb{R}^2$. Our approach copes with adaptive input, similar to the PointNet architecture [12]. Moreover, the network has to consider that the measurements never fully correspond to the extracted map landmarks due to the dynamic environment and measurement noise.

B. Objective

Our objective is to minimize the difference between the predicted $[\Delta \hat{x}, \Delta \hat{y}, \Delta \hat{\phi}]$ and ground-truth pose offsets $[\Delta x, \Delta y, \Delta \phi]$. We define the translation and rotation loss terms that are treated independently. The reason is the different units, i.e. meters and degree, that require scaling the two terms for equal gradient contribution. At first, the translation loss is given by:

$$L_{tran} = \mathbb{E}[(\Delta \hat{x} - \Delta x)^2] + \mathbb{E}[(\Delta \hat{y} - \Delta y)^2]. \quad (3)$$

Secondly, the rotation loss is defined as:

$$L_{rot} = \mathbb{E}[(\Delta \hat{\phi} - \Delta \phi)^2]. \quad (4)$$

We found that manually tuning the weighting of the two terms to be a tedious task. Furthermore, the weights can be sensitive to small modifications in the training data. Rather than choosing a data specific weighting strategy, we learn the weighting factors. The complete loss function is defined as:

$$L = L_{tran} e^{-s_{tran}} + s_{tran} + L_{rot} e^{-s_{rot}} + s_{rot}, \quad (5)$$

where $s_{tran} = \log \sigma_{tran}^2$ and $s_{rot} = \log \sigma_{rot}^2$. The terms σ_{tran} and σ_{rot} denote the homoscedastic uncertainty, derived from Bayesian modeling. Homoscedastic uncertainty is a subtype of aleatoric uncertainty that is not dependent on the input data. It is therefore constant but varies between different tasks. Following [24], homoscedastic uncertainty can be interpreted as task-dependent weighting, which can be learned

by the network. In our formulation, the tasks correspond to the translation and rotation. Our loss function is similar to the geometric loss function in [25], where the only difference is the pose degrees of freedom.

C. Network Architecture

DeepLocalization, our network architecture, is presented in Fig. 2. The inputs of DeepLocalization are two independent point lists, namely the measurements and map landmarks. For each of the two input lists we employ a separate MLP with three layers, denoted by MLP_{meas} and MLP_{map} in Fig. 2, which transform the input to a higher dimensional representation \mathbb{R}^D , where $D = 1024$. Note that the weights of MLP_{meas} are shared for every measurement, similar for the map landmarks and MLP_{map} . The output of each MLP is $\nu \times 1024$ for the measurements and $\mu \times 1024$ for the map landmarks. At the end of MLP_{meas} and MLP_{map} , a max-pooling operation follows to produce the global feature vector of D elements. One can observe that the global feature vector does not depend on the number of input landmarks which makes the network invariant to the input size. In addition, the global feature vector is invariant to input permutations [12]. Finally, the two global feature vectors are concatenated and fed to a third $\text{MLP}_{\text{offset}}$. The role of $\text{MLP}_{\text{offset}}$ is to find the correlation between the measurements and map landmarks, which now have been projected to the same dimensions. The output of $\text{MLP}_{\text{offset}}$ is the vehicle's pose offset.

It's important to note that the map landmarks are loaded only for a radius of 100m around the vehicle's position. During training, we do have the ground-truth information for the vehicle's location and, consequently we can load the corresponding map landmarks. During testing, we make use of the previous or initial vehicles location to load the map landmarks. Although, the test radius is slightly delayed in time, we have empirically found that it does not have any negative impact on the pose offset prediction.

D. Training Process

The training of our model is based on simulating the pose offsets. We randomly fetch from the training data the following: the vehicle's ground-truth pose in the UTM coordinate system $\mathbf{p}_{\text{UTM}} = [x_{\text{UTM}}, y_{\text{UTM}}, \phi_{\text{UTM}}]$, the map landmarks $\{\mathbf{m}_1, \dots, \mathbf{m}_\mu\}$ in the UTM coordinate system and the measurements $\{\mathbf{z}_1, \dots, \mathbf{z}_\nu\}$ in the vehicle's coordinate system. In addition, we randomly sample a pose offset $[\Delta x, \Delta y, \Delta \phi]_{\sigma_x, \sigma_y, \sigma_\phi}$ from a uniform distribution on the interval $\Delta x \in [-\sigma_x, \sigma_x]m$, $\Delta y \in [-\sigma_y, \sigma_y]m$ and $\Delta \phi \in [-\sigma_\phi, \sigma_\phi]^\circ$. The pose offset composes the desired network output, i.e. ground-truth, and is applied to the vehicle's pose at the UTM coordinate system such that it causes a shift. This is written as:

$$\hat{\mathbf{p}}_{\text{UTM}} = \mathbf{p}_{\text{UTM}} + [\Delta x, \Delta y, \Delta \phi]_{\sigma_x, \sigma_y, \sigma_\phi}^T, \quad (6)$$

where $\hat{\mathbf{p}}_{\text{UTM}} = [\hat{x}_{\text{UTM}}, \hat{y}_{\text{UTM}}, \hat{\phi}_{\text{UTM}}]$. Based on the shifted vehicle's pose in the UTM coordinate system, we define the homogeneous transformation matrix H that transforms

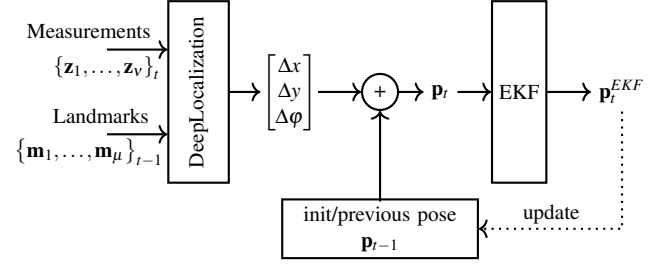


Fig. 3. Overview of filter-based system architecture. The output of the network is applied to an initial or previous localization result. The corrected pose is the input measurement for an EKF with constant turn rate and velocity motion model. Therefore, the EKF predicts a smoothed pose based on the previous pose and the network output, which is used for the next time-step.

a measurement from the vehicle's to the UTM coordinate system. This is given by:

$$H = \begin{bmatrix} \cos(\hat{\phi}_{\text{UTM}}) & -\sin(\hat{\phi}_{\text{UTM}}) & \hat{x}_{\text{UTM}} \\ \sin(\hat{\phi}_{\text{UTM}}) & \cos(\hat{\phi}_{\text{UTM}}) & \hat{y}_{\text{UTM}} \\ 0 & 0 & 1 \end{bmatrix}. \quad (7)$$

We can use H to transform all measurements to the UTM coordinate system. However, we perform the opposite by transforming the map landmarks to the vehicle's coordinate system with the inverse transformation matrix H^{-1} for numerical stability reasons. The range of values in the vehicle's coordinate system is better suited for training a neural network. Moreover, we predict offsets, i.e. translation and rotation, which are independent from the coordinate system. At this point, the map landmarks and the measurements are in the vehicle's coordinate system.

This procedure allows us, theoretically, to generate infinite amount of training data. Moreover, the sampling order over time does not play any role in our optimization. Thus, we can sample training data at random time-steps.

IV. INFERENCE

We present two different inference approaches. First, the GPS-based inference is based on improving the GPS sensor measurement at every-time step. Second, the filter-based inference where we combine our approach with an extended Kalman filter (EKF) to make use of the temporal information.

A. GPS-based Inference

The first inference algorithm relies on the GPS measurement for obtaining an initial but noisy vehicle pose. Here, we do not make use of the previous time-step pose. Thus, we rewrite Eq. (2) as:

$$\mathbf{p}_t = \mathbf{p}_{\text{GPS}} + [\Delta \hat{x}, \Delta \hat{y}, \Delta \hat{\phi}]^T, \quad (8)$$

where \mathbf{p}_{GPS} is the noisy GPS vehicle pose in the UTM coordinate system. To obtain the pose offsets $\Delta \hat{x}$, $\Delta \hat{y}$ and $\Delta \hat{\phi}$ from DeepLocalization, we follow the same pipeline as in the training process from Sec. III-D. The loaded map landmarks are transformed to the vehicle's coordinate system based on H^{-1} , where the position and orientation from \mathbf{p}_{GPS} are used in H . The same process is followed at every time-step to estimate \mathbf{p}_t .



Fig. 4. Overview of the landmark-based map with landmarks depicted as red circles (●). The route in Ulm-Lehr (Germany) is about 5km long and is comprised of 3860 map landmarks.

B. Filter-based Inference

The filter-based algorithm requires an initial position, which can be retrieved from the GPS sensor. We rely on Eq. (2) to predict the vehicle's position in the UTM coordinate system. At time-step t , the measurements become available in the vehicle's coordinate system. Moreover, the map landmarks are loaded based on the previous vehicle pose \mathbf{p}_{t-1} . The map landmarks are expressed in the vehicle's coordinate system by applying the transformation H^{-1} . The transformation H^{-1} is computed from the previous vehicle pose \mathbf{p}_{t-1} , as \mathbf{p}_t is not available. Measurements and map landmarks in the vehicle's coordinate system are provided to DeepLocalization to regress the pose offset $[\Delta\hat{x}, \Delta\hat{y}, \Delta\hat{\phi}]$. Then, the new vehicle pose \mathbf{p}_t is estimated by applying the regressed offset to \mathbf{p}_{t-1} .

Nevertheless, our network does not take into consideration the time domain, which could help to avoid pose drifts. To address this issue, we additionally propose to combine our network with an EKF that has a constant turn rate and velocity (CTRV) motion model. The EKF takes the new vehicle pose \mathbf{p}_t , i.e. Eq. (2), and refines it such that

$$\mathbf{p}_t^{EKF} = EKF(\mathbf{p}_t), \quad (9)$$

where EKF represents the filter. At the next time-step, the pose \mathbf{p}_t^{EKF} is used as \mathbf{p}_{t-1} and the process is repeated with new measurements. An overview of the filter-based inference method is shown in Fig. 3.

V. ULM-LEHR DATASET AND MAP CREATION

We introduce our dataset to examine DeepLocalization in real-world scenarios. To that end, we have made recordings with our vehicle, equipped with stereo camera, laser and radar sensors, as well as a dGPS system for generating the ground-truth vehicle's pose. Our test track is Ulm-Lehr (Germany), which is about 5km long, can be seen in Fig. 4 along with the landmarks from the map.

The landmark-based map has been created in December 2017 by recording three runs on different days at our test track in Ulm-Lehr. It consists of 3860 landmarks, of which 1731 were obtained from laser measurements, 1411 from camera images and 718 from radar targets. Independently, the dataset has been built from eight runs on the Ulm-Lehr route in November 2018. In total, the dataset includes approximately 145.000 samples. Six runs (105.000 samples) are used for the training and validation. The remaining two runs (40.000 samples) are used for test. Below, we discuss in detail the landmark extraction process and the generation of the landmark-based map.

A. Landmark Extraction

All measurement recordings take place with the same sensor configuration. While driving the route, we record measurements in the form of 3D point clouds for the laser and radar sensors; and RGB image and depth from the stereo system. We extract features from raw measurements because we found them to be more stable and computationally efficient. For the laser and radar measurements, the density based DBSCAN [26] cluster algorithm is applied to group adjacent points that have a minimum amount of neighboring points within a predefined distance. For the RGB images, stable extremal regions (MSER) [27] features are extracted. The MSER algorithm is parameterized to detect road markings since they are permanent and thus can be detected recurrently. All features are stored in the vehicle's coordinate system that has the origin at the center of the rear axle. The image features, in particular, are transformed to the vehicle's coordinate system using the depth map. The extracted features from laser, radar and RGB image define what we call landmarks. Additionally, the dGPS system records the ground-truth pose of the vehicle. It consists of the latitude and longitude coordinates that are transformed into Cartesian coordinates (UTM); and the heading (yaw) orientation.

B. Landmark-based Map

The landmark extraction process (Sec. V-A) is sufficient for extracting landmarks as measurements, but it is not enough for building our map. There are several landmark instances that are repeated several times. To avoid storing the same landmark multiple times, we rely on the LMB-SLAM algorithm [10] to make the landmark-based map sparser. In addition, dynamic objects, such as vehicles or time-dependent structures, may produce landmarks which are not valid for future use. To discard this type of landmarks, we fuse all three runs from December 2017 with a Bernoulli filtering approach [28]. Finally, the map landmarks are expressed in the UTM coordinate system. We have transformed the landmarks from the vehicle's to the UTM coordinate system by incorporating the dGPS measurements. Therefore, the map landmarks have a relative accuracy of a few centimeters.

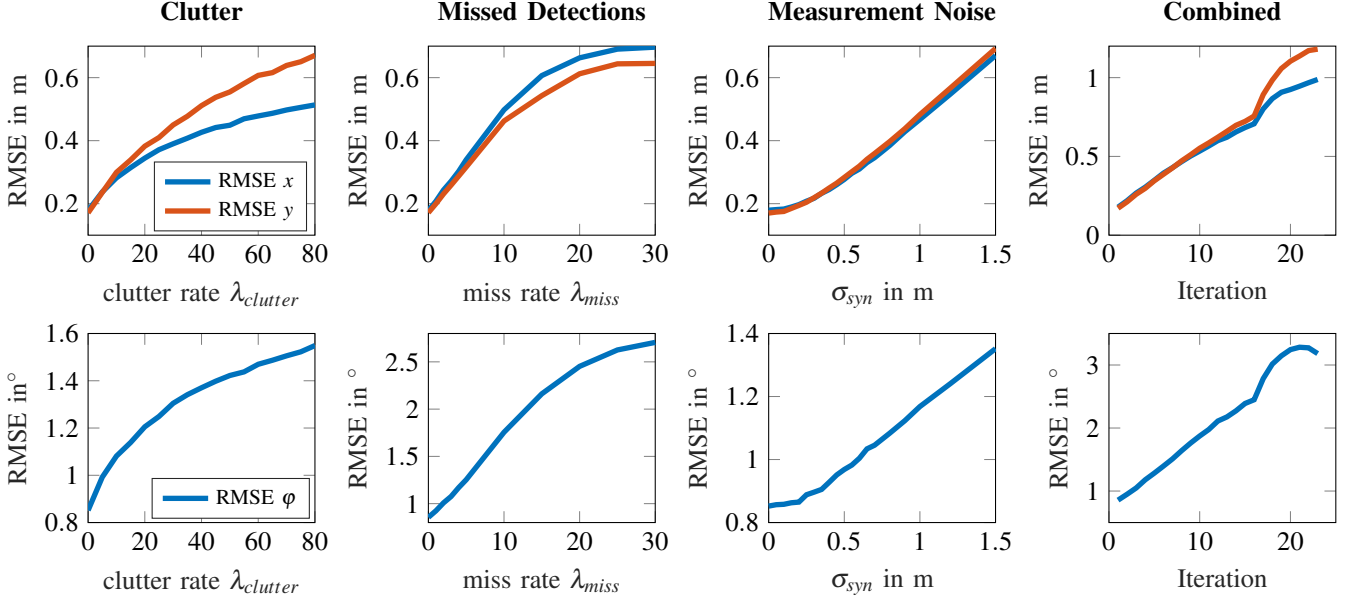


Fig. 5. Overview of simulation results. The first row depicts the RMSE results of the position and the bottom row shows the RMSE results of the orientation. In the first experiment, poisson distributed clutter is added with $\lambda_{clutter} \in [0, 80]$ (first column). Measurements are deleted in the second experiment, with deletion rate $\lambda_{miss} \in [0, 30]$ (second column). In the third experiment, noise is sampled randomly from a uniform distribution on the interval $[-\sigma_{syn}, \sigma_{syn}]$ with $\sigma_{syn} \in [0, 1.5]$ m (third column). The last experiment shows the result of the simulation, where all three effects occur simultaneously and are increased incrementally (fourth column).

VI. EXPERIMENTS

We conduct two experiments on the Ulm-Lehr dataset to evaluate our approach. First, we examine our model with simulated measurements and pose offsets. Second, we evaluate on the test set and compare our results with prior work. For all experiments, we rely on the same DeepLocalization model, which has a total of 1.8 million learn-able parameters. Our model has been trained with the ADAM optimizer, where the batch size has 500 samples and the learning rate is 10^{-5} . Additionally, all MLP networks have dropout [29] after every layer as regularizer, except the last one. During test, the inference time is 1.758 ms. Our approach is implemented in *TensorFlow* [30] and all operations are performed on a *Nvidia GeForce 1080Ti*. Furthermore, the map has a size of about 600 kB.

A. Synthetic Vehicle Pose Offset Evaluation

We extract the map landmarks for each sample of the Ulm-Lehr dataset to examine the lower error bound of our approach. Furthermore, we access how DeepLocalization generalizes under error-prone, missing or additional measurements.

First, we investigate the minimum error which we could achieve when using correct measurements. For each time-step, the map landmarks in the vehicle’s field of view are used as measurements too. When the measurements and map landmarks are identical, the input is ideal and the only source of error can be the incorrect offset prediction of our network.

To examine the above assumption, we transform the measurements and map landmarks to the vehicle’s coordinate system. Then, a synthetic vehicle pose offset is added to the

map landmarks as in training, Eq. (6). To generate the vehicle pose offset, we sample noise uniformly on the interval $\sigma_x, \sigma_y \in [-2, 2]$ m and $\sigma_\phi \in [-10, 10]^\circ$. We train our model based on the synthetic pose offsets. During test, our network receives the measurements and shifted map landmarks to predict the pose offset. Since the ground-truth is the synthetic vehicle pose offset, we can measure the prediction accuracy with the RMSE metric. We generate around 40.000 test samples and achieve a RMSE of 0.178 m and 0.17 m for the x and y coordinates, respectively. Furthermore, the orientation error is 0.852° . The results are also summarized in Tab. I. Next, we consider the following situations:

- 1) randomly delete measurements (simulating missed landmarks)
- 2) randomly add measurements (simulating clutter)
- 3) add randomly sampled noise to each measurement (simulating sensor noise)
- 4) we evaluate our network by adding all three impairments simultaneously.

In practice, the rates at which measurements are added and deleted follow a Poisson distribution $P_\lambda(k) = \lambda^k \exp(-\lambda)/(k!)$, where λ is the average number of events. The measurement noise for the third experiment is sampled from a uniform distribution on the interval $[-\sigma_{syn}, \sigma_{syn}]$. The evaluations are performed by increasing λ and σ_{syn} . Our results are presented in Fig. 5.

One can observe that with clutter rates of $\lambda_{clutter} = 40$, the error remains low at 0.4 m, even though the average number of actual measurements is about 20–30 per time step. Similar results are observed for missed detections with $\lambda_{miss} = 10$ and uniformly sampled noise for every landmark of about

TABLE I
RESULTS FOR SIMULATION AND REAL-WORLD SCENARIO.

Experiment	x	RMSE y	ϕ	inference time
Synthetic Pose Offset:				
DeepLocalization $\sigma_{xy} = 2\text{ m}, \sigma_{\phi} = 10^\circ$	0.178 m	0.170 m	0.852°	1.758 ms
GPS-based Inference:				
DeepLocalization $\sigma_{xy} = 2\text{ m}, \sigma_{\phi} = 10^\circ$	0.773 m	0.701 m	2.52°	1.771 ms
DeepLocalization $\sigma_{xy} = 1\text{ m}, \sigma_{\phi} = 4^\circ$	0.447 m	0.377 m	1.37°	1.761 ms
DeepLocalization $\sigma_{xy} = 0.5\text{ m}, \sigma_{\phi} = 2^\circ$	0.276 m	0.231 m	0.85°	1.728 ms
Filter-based Inference:				
DeepLocalization + EKF $\sigma_{xy} = 1\text{ m}, \sigma_{\phi} = 4^\circ$	0.566 m	0.339 m	1.26°	2.133 ms
DeepLocalization + EKF + GPS $\sigma_{xy} = 1\text{ m}, \sigma_{\phi} = 4^\circ$	0.271 m	0.245 m	0.82°	2.374 ms
RFS-MCL + GPS [11]	0.287 m	0.264 m	1.99°	28.92 ms

$\sigma_{syn} \in [-0.9, 0.9]\text{ m}$. Finally, the robustness of our approach is demonstrated when all three impairments occur simultaneously. For instance, in iteration 10 ($\lambda_{clutter} = \lambda_{miss} = 10$ and $\sigma_{syn} = 0.27\text{ m}$) the RMSE value for x and y is about 0.55 m and for the orientation 1.87°.

B. Real-World Evaluation

For this experiment, we train our network with the measurements and map landmarks of the Ulm-Lehr train set. To examine the robustness of our approach, we first generate synthetic noise offsets to train three network baselines. For the first baseline, we sampled noise from a uniform distribution on the interval $\sigma_x \in [-2, 2]\text{ m}$, $\sigma_y \in [-2, 2]\text{ m}$ and $\sigma_{\phi} \in [-10, 10]^\circ$. For the second baseline, the noise is sampled from the interval $\sigma_x \in [-1, 1]\text{ m}$, $\sigma_y \in [-1, 1]\text{ m}$ and $\sigma_{\phi} \in [-4, 4]^\circ$; and the sampled noise for the last baseline was on the interval $\sigma_x \in [-0.5, 0.5]\text{ m}$, $\sigma_y \in [-0.5, 0.5]\text{ m}$ and $\sigma_{\phi} \in [-2, 2]^\circ$. In all three experiments, we use GPS-based inference in order to improve the localization over the noisy GPS measurement. The results are summarized in Tab. I.

Next, we evaluate the filter-based inference using the EKF. Here we have relied on a single GPS measurement to initialize the algorithm. Our prediction offset has updated the vehicle pose from time-step $t - 1$ to t . After evaluating the three baselines, we have concluded that the baseline with $\sigma_x = 1\text{ m}$, $\sigma_y = 1\text{ m}$, $\sigma_{\phi} = 4^\circ$ performs at best when combined with the EKF with accuracies (RMSE) of 0.566 m and 0.339 m for the x and y position, respectively. Thus, we only report these result in Tab. I.

Furthermore, we compare our approach with the Monte-Carlo localization (MCL) method that uses the same map and features, derived from the multi-modal measurements [11]. Unlike our learning-based approach, Stuebler *et al.* have

modeled the measurements and landmarks as Random Finite Sets (RFS), combined with a particle filter. The weights of the particles are updated using a bernoulli filtering approach. An in-depth explanation of the RFS MCL method can be found in [11]. We have re-implemented their approach with a total of 1000 particles which translates to 28.92 ms of inference time. In our implementation, the method builds on additional GPS measurements. For that reason, we also evaluate results by incorporating GPS measurements in the EKF filter. With this, we achieve position accuracies (RMSE) in the range of 0.245 m – 0.271 m and an orientation accuracy of 0.82°. Our approach has a computational time of 2.374 ms, which is about ten times faster than the traditional RFS MCL. Finally, a visual illustration of DeepLocalization with an EKF is shown in Fig. 6. It becomes apparent that our prediction is very close to the ground-truth position in the UTM coordinate system.

VII. CONCLUSION

In this work, we have proposed a new approach for vehicle self-localization. We have introduced DeepLocalization, a deep neural network that copes with dynamic input from the measurements and map landmarks. Our network learns to predict the vehicle's pose from measurements and map landmarks. We have presented two inference algorithms, namely GPS-based and filter-based inference. In the evaluation, we have shown better performance than the prior work on the Ulm-Lehr dataset. Moreover, our approach runs ten times faster than the related work. Finally, we have demonstrated that DeepLocalization is complementary to filtering approaches such as an EKF. As future work, we would like to explore how to be independent of GPS measurements.

REFERENCES

- [1] S. Thrun, W. Burgard, and D. Fox, *Probabilistic robotics*. MIT press, 2005.
- [2] F. Kunz, *et al.*, "Autonomous driving at ulm university: A modular, robust, and sensor-independent fusion approach," in *2015 IEEE intelligent vehicles symposium (IV)*. IEEE, 2015, pp. 666–673.
- [3] F. Gies, A. Danzer, and K. Dietmayer, "Environment perception framework fusing multi-object tracking, dynamic occupancy grid maps and digital maps," in *2018 21st International Conference on Intelligent Transportation Systems (ITSC)*. IEEE, 2018, pp. 3859–3865.
- [4] A. Mohamed and K. Schwarz, "Adaptive kalman filtering for ins/gps," *Journal of geodesy*, vol. 73, no. 4, pp. 193–203, 1999.
- [5] T. Kos, I. Markezic, and J. Pokrajic, "Effects of multipath reception on gps positioning performance," in *Proceedings ELMAR-2010*. IEEE, 2010, pp. 399–402.
- [6] M. Cummins and P. Newman, "Fab-map: Probabilistic localization and mapping in the space of appearance," *The International Journal of Robotics Research*, vol. 27, no. 6, pp. 647–665, 2008.
- [7] J. Ziegler, *et al.*, "Video based localization for berth," in *Intelligent Vehicles Symposium Proceedings, 2014 IEEE*. IEEE, 2014, pp. 1231–1238.
- [8] M. A. Brubaker, A. Geiger, and R. Urtasun, "Map-based probabilistic visual self-localization," *IEEE transactions on pattern analysis and machine intelligence*, vol. 38, no. 4, pp. 652–665, 2016.
- [9] J. Wiest, *et al.*, "Localization based on region descriptors in grid maps," in *2014 IEEE Intelligent Vehicles Symposium Proceedings*. IEEE, 2014, pp. 793–799.
- [10] H. Deusch, S. Reuter, and K. Dietmayer, "The labeled multi-bernoulli slam filter," *IEEE Signal Processing Letters*, vol. 22, no. 10, pp. 1561–1565, 2015.

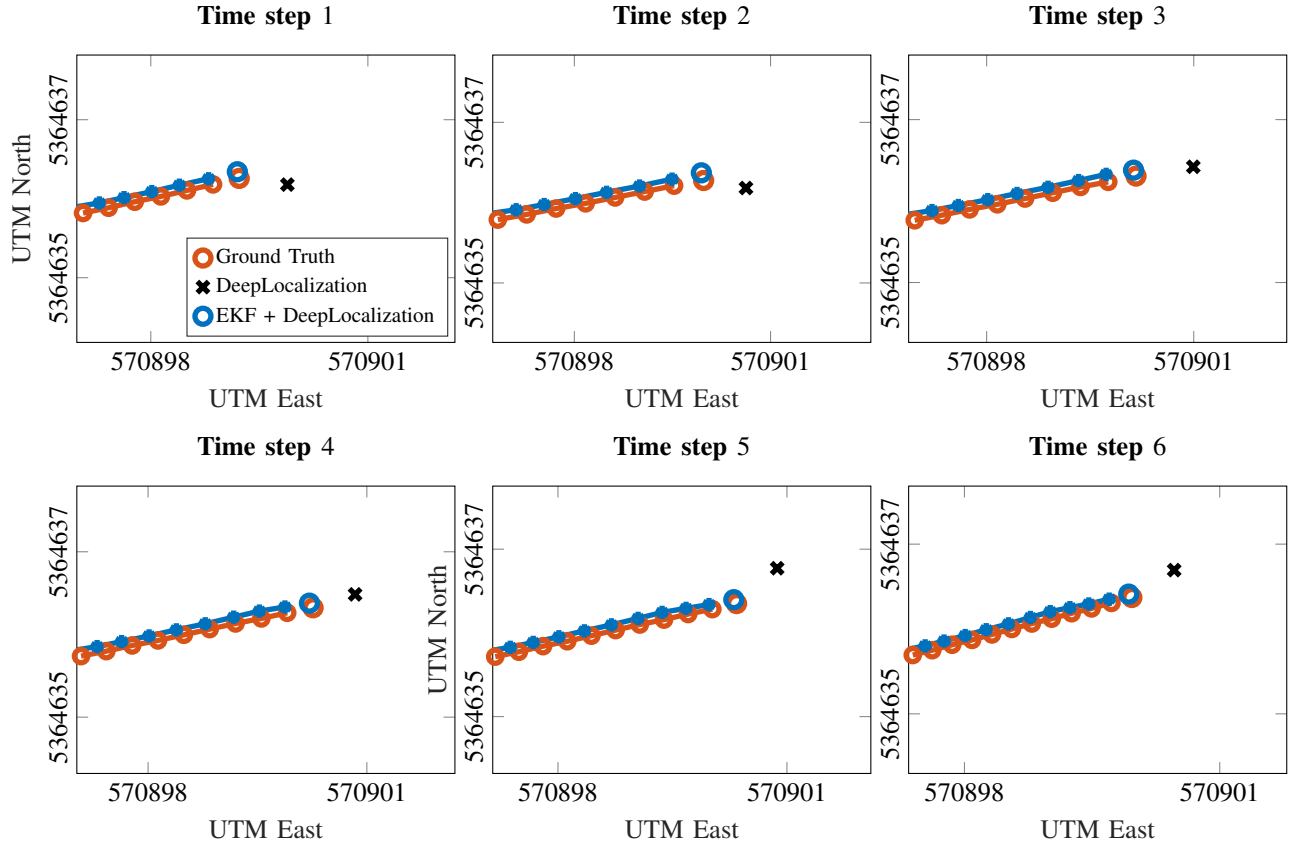


Fig. 6. Exemplary sequence of DeepLocalization results in combination with the EKF. We show six consecutive samples with the preceding ground truth and predicted trajectory. Results of our network are depicted as a black cross and the smoothed output of the EKF as a blue circle. Although the network was trained with random noise, it generalizes to real-world applications and corrects the pose from the previous result in the correct direction. Small errors are adjusted by the EKF with an underlying CTRV motion model.

- [11] M. Stuebler, "Self-assessing localization and long-term mapping using random finite sets," Ph.D. dissertation, Ulm University, 2018. [Online]. Available: <https://oparu.uni-ulm.de/xmlui/handle/123456789/10740>
- [12] C. R. Qi, H. Su, K. Mo, and L. J. Guibas, "Pointnet: Deep learning on point sets for 3d classification and segmentation," *Proc. Computer Vision and Pattern Recognition (CVPR)*, IEEE, vol. 1, no. 2, p. 4, 2017.
- [13] F. Dellaert, D. Fox, W. Burgard, and S. Thrun, "Monte carlo localization for mobile robots," in *ICRA*, vol. 2, 1999, pp. 1322–1328.
- [14] S. Thrun, D. Fox, W. Burgard, and F. Dellaert, "Robust monte carlo localization for mobile robots," *Artificial intelligence*, vol. 128, no. 1-2, pp. 99–141, 2001.
- [15] J. Levinson, M. Montemerlo, and S. Thrun, "Map-based precision vehicle localization in urban environments," in *Robotics: Science and Systems*, vol. 4. Citeseer, 2007, p. 1.
- [16] J. Levinson and S. Thrun, "Robust vehicle localization in urban environments using probabilistic maps," in *2010 IEEE International Conference on Robotics and Automation*. IEEE, 2010, pp. 4372–4378.
- [17] R. W. Wolcott and R. M. Eustice, "Fast lidar localization using multiresolution gaussian mixture maps," in *Robotics and Automation (ICRA)*, 2015 *IEEE International Conference on*. IEEE, 2015, pp. 2814–2821.
- [18] P. J. Besl and N. D. McKay, "Method for registration of 3-d shapes," in *Sensor Fusion IV: Control Paradigms and Data Structures*, vol. 1611. International Society for Optics and Photonics, 1992, pp. 586–607.
- [19] A. Segal, D. Haehnel, and S. Thrun, "Generalized-icp," in *Robotics: science and systems*, vol. 2, no. 4, 2009, p. 435.
- [20] R. Kümmerle, R. Triebel, P. Pfaff, and W. Burgard, "Monte carlo localization in outdoor terrains using multilevel surface maps," *Journal of Field Robotics*, vol. 25, no. 6-7, pp. 346–359, 2008.
- [21] A. Kendall, M. Grimes, and R. Cipolla, "Posenet: A convolutional network for real-time 6-dof camera relocalization," in *Proceedings of the IEEE international conference on computer vision*, 2015, pp. 2938–2946.
- [22] A. Valada, N. Radwan, and W. Burgard, "Deep auxiliary learning for visual localization and odometry," in *2018 IEEE International Conference on Robotics and Automation (ICRA)*. IEEE, 2018, pp. 6939–6946.
- [23] L. Ding and C. Feng, "Deepmapping: Unsupervised map estimation from multiple point clouds," *arXiv preprint arXiv:1811.11397*, 2018.
- [24] A. Kendall, Y. Gal, and R. Cipolla, "Multi-task learning using uncertainty to weigh losses for scene geometry and semantics," in *Proceedings of the IEEE Conference on Computer Vision and Pattern Recognition*, 2018, pp. 7482–7491.
- [25] A. Kendall, R. Cipolla, et al., "Geometric loss functions for camera pose regression with deep learning," in *Proc. CVPR*, vol. 3, 2017, p. 8.
- [26] M. Ester, H.-P. Kriegel, J. Sander, X. Xu, et al., "A density-based algorithm for discovering clusters in large spatial databases with noise," in *Kdd*, vol. 96, no. 34, 1996, pp. 226–231.
- [27] J. Matas, O. Chum, M. Urban, and T. Pajdla, "Robust wide-baseline stereo from maximally stable extremal regions," *Image and vision computing*, vol. 22, no. 10, pp. 761–767, 2004.
- [28] M. Stuebler, S. Reuter, and K. Dietmayer, "A continuously learning feature-based map using a bernoulli filtering approach," in *2017 Sensor Data Fusion: Trends, Solutions, Applications (SDF)*. IEEE, 2017, pp. 1–6.
- [29] N. Srivastava, G. Hinton, A. Krizhevsky, I. Sutskever, and R. Salakhutdinov, "Dropout: a simple way to prevent neural networks from overfitting," *The Journal of Machine Learning Research*, vol. 15, no. 1, pp. 1929–1958, 2014.
- [30] M. Abadi, et al., "TensorFlow: Large-scale machine learning on heterogeneous systems," 2015, software available from tensorflow.org. [Online]. Available: <https://www.tensorflow.org/>